SSRG International Journal of Mechanical Engineering
ISSN: 2348-8360/ https://doi.org/10.14445/23488360/IJME-V13I2P106

Volume 13 Issue 2, 63-78, February 2026

Original Article

Investigation of the Effect of Infill Pattern of 3D Printed PLA Components on Tensile and Flexural Properties through Experimentation and SEM

T Venkategowda[1], Prashanth Kumar Sanjeevaiah[1], Anilkumar P R[2]

[1]*Department of Mechanical Engineering, Seshadripuram Institute of Technology, Karnataka, India.*
[2]*Department of Mechanical Engineering, Sapthagiri NPS University, Karnataka, India.*

[1]*Corresponding Author : venkategowda.t@sitmysore.ac.in*

Received: 24 November 2025 Revised: 26 December 2025 Accepted: 25 January 2026 Published: 20 February 2026

Abstract - *The study investigates the mechanical properties of the fifteen components having different infill patterns produced using Polylactic Acid (PLA) and Fused Filament Fabrication (FFF) technique. According to ASTM standards, the tensile and flexural testing were conducted, which showed that the honeycomb design has the best overall mechanical performance. Infill density, printing speed, layer height, and nozzle temperature are the factors considered for optimization through Response Surface Methodology. The optimal parameters resulting in increased tensile and flexural properties are infill density of 30%, print speed of 75.43 mm/s, layer height of 0.1029 mm, and nozzle temperature of 218.74 °C. The statistical models used are highly significant (R^2>0.95). Further, Scanning Electron Microscopy (SEM) is used to provide insight into the fracture mechanism, which validated the behaviour of the materials observed during testing. This combined experimental/analytical methodology provides a valuable approach to identify the best combination of infill patterns to achieve the desired mechanical properties in PLA parts fabricated using the FFF technique.*

Keywords - *Fused Filament Fabrication, Infill Pattern, Mechanical properties, Response Surface Methodology, Scanning Electron Microscopy.*

1. Introduction

Additive Manufacturing (AM), frequently termed 3D printing, has seen a significant rise in attention over the past few years due to two key factors: a growing number of smaller companies utilizing AM technologies to create prototypes quickly, and the accompanying introduction and wide availability of inexpensive AM systems that provide people with the means of making unique high-quality items from their residence/place of work [1]. Out of all types of AM processes currently available, Fused Filament Fabrication (FFF) is the most widely used method. FFF is considered to be affordable, is reliant to a large extent on inexpensive materials, and can be operated [2]. The FFF process allows the user to create physical objects from their digital representations through the use of three-dimensional Computer-Aided Design (CAD) drawings. The deposition of material layer by layer is achieved through FFF by using the G-codes developed using the CAD model of the component. In addition to this, since FFF is a near-net-shape manufacturing method, it also allows for the production of very complex shapes, while creating very little waste in terms of both material and tooling [3].

The FFF process begins with a 3D model of the desired component. The component gets sliced into discrete layers using slicing programme software (usually STL format), before it can be printed. Since FFF printers cannot interpret continuous geometry as it is developed in the design process, the slicing software will generate G-code (a sequence of instructions to the printer) to elaborate those instructions as they apply to the extrusion speed, travel rate, and sequence of layers for the printing process [4]. This data will provide the printing apparatus with the necessary information to enable the fusing of each layer to form the completed part.

2. Literature Review

The FFF printed part will have an outside shell and an internal structure that will represent the majority of the volume of the printed part. The mechanical strength, stiffness, weight, print time, and material consumption of the finished item are determined by the volume of the internal structure. The density of an FFF printed part's internal structure (calculated as the percentage of solid material versus void space) will range between 0% (a hole) to 100% (solid), while the majority of FFF printed parts will have an internal structure density between 30% and 50%, which Typically maximises the

mechanical characteristics and the cost-effectiveness of the final product [5]. Maintaining the density of the filling material (as long as the filling density is greater than 0%) will increase the stiffness and strength of the part; however, the production time and material utilisation will likewise increase. The production of an FFF printed part with 100% filling density is rarely practical, considering the time and cost considerations associated with producing FFF printed parts [6-8].

Fill density is only one factor that influences the mechanical characteristics of an FFF printed part; fill geometry has likewise been proven to affect the way loads are transferred, how stress is distributed, and deflection of the part occurs during load-bearing applications. Studies have demonstrated that the mechanical behaviour of an FFF printed part will differ with the changing of line fill patterns (with no change in fill density). For instance, the mechanically tested FFF printed parts with hexagonal fill patterns exhibited higher ultimate tensile strength when compared with fill patterns using geometric grid or triangular patterns of line fill when all were printed using the same fill density [9], there is significant variability in the mechanical behaviour of FFF printed parts using line fill patterns with consistent fill densities when testing under controlled conditions [10]. Similarly, when the geometry of fill is altered, the ultimate tensile strength of the filled part is also altered, thus exemplifying the importance of fill geometry selection in the design of FFF printed parts [11].

The internal geometric layout of infill materials and the kind of infill pattern are key determinants for load transfer, stress distribution, and deformation characteristics of 3D printed parts at a given infill density. Recent research emphasizes that the changing infill geometries and constant infill density affect the mechanical behavior of the parts developed using 3D printing. Hexagonal shapes provide higher tensile strength than grid or triangular built structures at an equal infill density, while the differences in strength and resiliency of commonly used patterns are documented under controlled conditions [9, 10]. Moreover, when studied as an independent variable, infill geometry has been illustrated to create significant variation in tensile behaviour, confirming the importance of choosing an appropriate pattern in FFF designs [11].

Beyond just tensile properties, the geometry of the infill last affects both stiffness and failure mechanisms. Grid patterns yield greater ultimate tensile strength compared to their counterpart honeycomb patterns, illustrating the variations between strength and stiffness based on pattern selection [12]. Higher density of the hexagonal infill patterns correlates with higher tensile Modulus and greater load-bearing capacity; therefore, geometry impacts both the strength and the modes of failure [13]. Therefore, infill pattern geometry impacts both strength and structural durability and the modes in which 3D printed parts fail. Once at the design level, weight-to-strength ratio, as well as the use of material per unit weight of strength, are important performance measurements when considering lightweight engineering applications.

It has been reported that hexagonal and rectilinear infill patterns consistently provide good weight-to-strength ratios, while rectilinear patterns provide for greater use of material at higher densities [10, 14]. These findings illustrate that infill density alone cannot be used to predict the performance of parts and that the geometric efficiency of the infill plays a central role in achieving mechanical efficiency.

Recent studies published between 2021 and 2025 indicate that both infill pattern and density of infill pattern significantly influence the mechanical properties of the parts fabricated using the FFF technique, as summarized in Table 1. In most cases, researchers are looking into a variety of different types of infill and generally only consider a few of these, somewhere between one and three. This means that it becomes harder to produce design guidelines that can be widely implemented. Also, many of the studies have primarily focused on different types of material enhancement methods, such as reinforced or composite filaments including PLA/CF, PLA/Cu, and other high-performance polymers such as PEEK; however, the emphasis has not focused on the systematic optimization of infill strategy or on the print time efficiency. As a result, the combined effects of geometric complexity, mechanical behaviour, and manufacturing efficiency are not thoroughly studied as per the existing research.

The considerable body of current literature on FFF printed parts focuses mostly on a limited number of infill patterns (1 to 3), which are typically measured with differing densities and orientations but do not address the systematic optimization of either the infill or the time to make such parts. As a result, most of these studies, which focus primarily on material enhancement strategies such as adding fiber reinforcement to the filament types, provide limited, large-scale, pattern-based design guidelines [15, 16].

Expanding the range of geometrical comparisons of various infill geometries would yield better information on the advantages and disadvantages of the geometries studied, and thus assist in making more informed design decisions. Systematic testing of the various geometries utilizing controlled testing conditions would provide a greater understanding of the relationships between strength, stiffness, and efficiency in selecting the best infill strategies for a specific application [10, 17, 18].

Furthermore, research comparing hybrid or combined patterns indicates that a combination of internal geometries will yield enhanced mechanical performance [19]. While experimental comparisons provide valuable insights, optimization of process parameters after identifying a

The promising infill pattern remains largely underexplored. The interactions between parameters such as density of infill, layer height, speed of printing, and temperature of extrusion are studied using Response Surface Methodology (RSM).

Also, RSM is used to predict the mechanical properties of FFF-printed parts [11, 18]. RSM-based optimization has further been shown to significantly enhance tensile and flexural performance by identifying optimal parameter combinations, yet its application following large-scale infill pattern comparisons remains limited [20].The research gap identified from the literature is the lack of a comprehensive, pattern-focused investigation that systematically evaluates a large number of commonly used infill geometries at a constant infill density, followed by statistical optimization of process parameters. This study focuses on:

1. The experimental evaluation of 15 commonly available infill patterns under identical printing conditions, enabling direct and unbiased comparison of their mechanical behavior.
2. The integration of RSM to optimize key process parameters for the best-performing infill pattern, thereby adopting a dual-phase approach that combines experimental benchmarking with statistical optimization.

This integrated methodology not only clarifies the isolated influence of infill pattern geometry but also provides practical design guidelines for achieving optimized strength, stiffness, and material efficiency in FFF-printed components-an approach that remains scarcely addressed in existing literature.

2.1. Problem Statement

The default settings available in the printer have limited the use of other infill pattern and their effect on the mechanical properties of the 3D printed parts. Because of this lack of clarity, many designs are inefficient and not optimised to provide maximum strength, flexibility, and material use.

The information about the change in the tensile and flexural properties of the 3D printed parts for various infill patterns is limited. There is also a need for a systematic approach to optimise the settings for printing once the optimal pattern has been determined.

2.2. Objectives

The specific objectives of this study are,

- To evaluate the impact of 15 different infill patterns on the tensile and flexural properties of components fabricated using the FFF technique and PLA material at a constant infill density.
- Identifying the best-performing infill pattern based on experimental testing according to ASTM standards.
- To perform failure analysis using Scanning Electron Microscopy (SEM) to investigate fracture morphology and understand the interlayer bonding behavior of samples.
- To apply RSM to optimize four process parameters, such as density of infill, layer height, speed of printing, and temperature of the nozzle for the selected pattern.
- To determine the optimal parameter combination to develop predictive models and maximize mechanical performance.

Table 1. Comparison of existing literature

Author	Objective	Material / Method	Infill Density	Outcomes	Limitations
Bardiya et al., 2021 [21]	Analyze effect of layer height, orientation, and infill % on flexural & tensile strength and time	PLA, FFF	20–80%	Max flexural: 40 MPa at 0.2 mm LH, 80% infill; Time reduced at 0.3 mm	Limited to 3 parametric variations
Ambati & Ambatipudi [22]	Study infill density & pattern on PLA strength	PLA, FFF	20–100%	Higher infill improved strength	No time or energy efficiency discussed
Hamoud et al. [23]	Analyze Cu-reinforced PLA on mechanical traits	PLA/Cu composite	-	Improved strength due to Cu content	Not focused on infill geometry or scaling
Öteyaka et al. [24]	Compare carbon fiber vs. pure PLA at different infill	PLA & PLA/CF	20–100%	Max flexural for PLA/CF 90 MPa at 100%	Pure PLA not as strong; No pattern comparison

Khodaee et al. [25]	Study multi-material ABS/PLA & parametric effects	ABS/PLA, FFF	20–100%	Flexural: ~35 MPa at 80%; tensile: up to 31 MPa	Focused on material mix, not infill optimization
Birosz & Andó [26]	Infill pattern scaling effect on strength vs. print time	PLA, FDM	75%	Max 2.4 mm V = 2282 N; Max 2960 N; Print time reduced by 30–40%	Not suitable for narrow features; only tensile tested
Balasubramanian et al. [27]	Evaluate strain rate and FDM parameters on tensile failure	PLA, FDM	-	Strain rate influenced failure mode	No infill pattern variation
Dhanapal et al. [28]	Dynamic mechanical properties of PEEK with infill patterns	PEEK, FFF	Grid, Triangular	Higher damping & storage modulus at 70–90% infill	High-end material (PEEK), not PLA
Kothandaraman et al. [29]	Characterization of PLA/CF with structured cell infill	PLA/CF	Cell-structured, variable geometry	High stiffness; application for aerospace	Complex infill, not practical for all printers
Karad et al. [30]	Study infill % impact on PLA flexural & tensile strength	PLA	Infill: 20–100%	80% infill flexural 48 MPa, tensile 30 MPa	No time/cost efficiency or scaling discussed

3. Methodology

The research starts with designing standard 3D testing samples, followed by selecting 15 separate infill patterns commonly used in FFF 3D printing. PLA samples are printed using each pattern under fixed processing conditions. Mechanical tests, including tensile and flexural evaluations, are conducted to determine the best-performing infill patterns. RSM is employed to analyze statistically and optimize four input parameters, such as infill density, printing speed, layer height, and nozzle temperature, to print the optimized pattern. The process aims to maximize output responses such as ultimate tensile strength, flexural strength, bending Modulus, and percentage elongation. The study concludes by proposing optimal parameter settings for extended mechanical performance Figure 1.

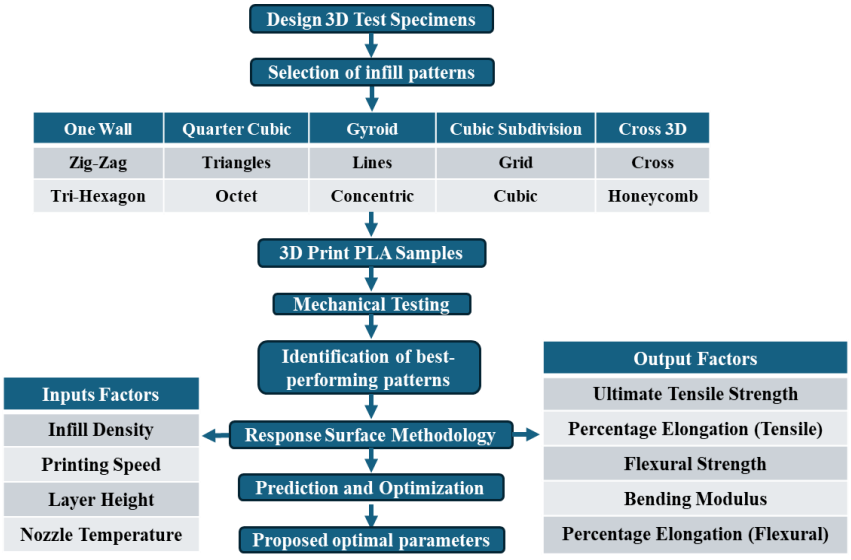

Fig. 1 Proposed research methodology

4. Sample Preparation

4.1. Materials

A filament having a 1.75mm diameter is selected due to its ease of use in FFF 3D printing technology, biodegradability, and In this study, PLA PRO+ filament is used as the base material for all 3D printed samples. PRO+ series PLA promising mechanical strengths.

The study focuses on analysing the effect on the mechanical properties, such as tensile and flexural strength due to different infill patterns used in producing the 3D printed components.

4.2. CAD Model Design

Standardized test specimens were created using CAD software, Onshape, as per the ASTM standard. Figures 2 and 3 show the 3D figures of the samples developed using CAD for 3D printing for the Tensile and Flexural testing.

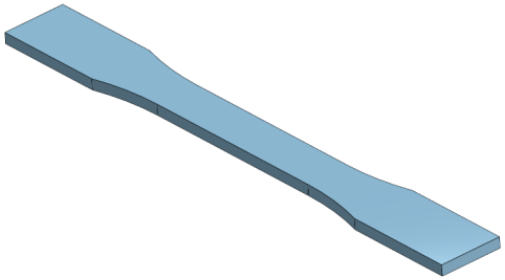

Fig. 2 3D CAD samples of tensile test

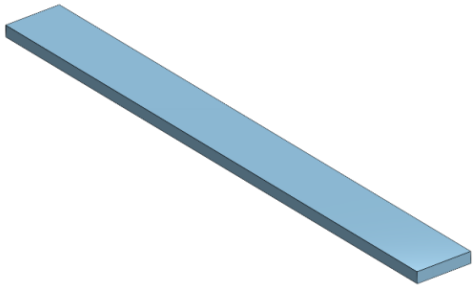

Fig. 3 3D CAD samples of flexural test

4.3. Fabrication of Test Samples

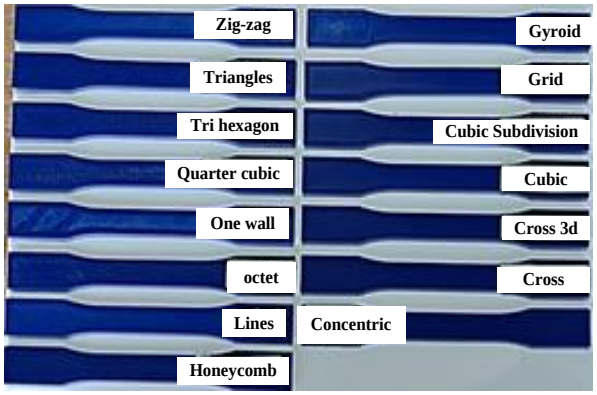

(a)

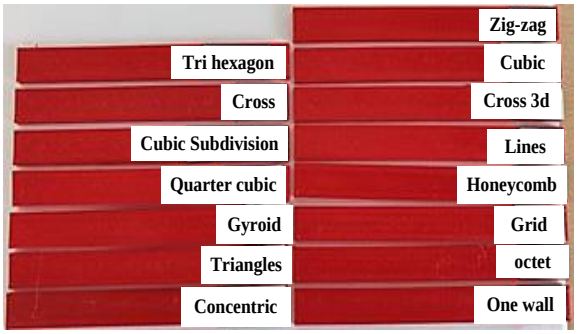

(b)

Fig. 4 3D printed PLA, (a) Tensile test specimens, and (b) Flexural test specimens.

Creality Ender-3 V3 KE is used to produce the 15 specimens through the Fused Filament Fabrication (FFF) technique for 15 different infill patterns shown in Figure 4 (a) & (b). The slicing software _Creality cloud' was used to generate a G-code file from a CAD model in order to make 3D printing. Each testing sample was printed at a constant infill density of 30% for 15 infill patterns. The standard printing parameters are shown in Table 2 to ensure consistency in printing. In Table 3, all types of infill patterns are listed and displayed. Also, for each infill pattern, the printing time and the amount of material consumed for each specimen are presented.

Table 2. Printing parameters

Printing Parameters	Value
Printing temperature	210 ºC
Bed temperature	60 ºC
Layer height	0.2mm
Printing speed	300mm/s
Travel speed	300mm/s
Initial Layer Speed	50mm/s
Wall Thickness	0.8mm
Infill density	30%
Infill pattern	Varied

Table 3. Estimated printing time and material for printing tensile and flexural specimens using commonly available infill patterns in creality cloud

Specimen No.	Infill Pattern	Tensile specimens		Flexural specimens	
		Estimated printing time	Estimated Material	Estimated printing time	Estimated Material
1	One wall	10Min 35Sec	1.83m	08Min 02Sec	0.99m
2	Zig-zag	12Min 50Sec	2.36m	08Min 50Sec	1.13m
3	Tri hexagon	12Min 54Sec	2.31m	09Min 19Sec	1.21m
4	Quarter cubic	12Min 55Sec	2.31m	09Min 24Sec	1.21m
5	Triangles	12Min 57Sec	2.31m	09Min 24Sec	1.21m
6	octet	12Min 58Sec	2.31m	09Min 25Sec	1.21m
7	Gyroid	14Min 04Sec	2.31m	10Min 58Sec	1.20m
8	Lines	14Min 35Sec	1.95m	08Min 59Sec	1.19m
9	Concentric	15Min 32Sec	2.31m	08Min 31Sec	1.15m
10	Cubic Subdivision	16Min 43Sec	2.30m	09Min 13Sec	1.16m
11	Grid	16Min 57Sec	2.37m	09Min 15Sec	1.18m
12	Cubic	17Min 07Sec	2.40m	09Min 21Sec	1.20m
13	Cross 3d	18Min 17Sec	2.29m	10Min 11Sec	1.20m
14	Cross	18Min 28Sec	2.35m	09Min 59Sec	1.19m
15	Honeycomb	31Min 44Sec	3.25m	15Min 16Sec	1.55m

5. Mechanical Testing

5.1. Tensile Test

ASTM D638 standard is used to conduct the specimen testing to determine the percent elongation and ultimate tensile strength of the specimens produced using 15 different infill patterns. As seen in Figure 4, 3D printed samples of 15 types of infill patterns are created for the tensile test. Tensile test is conducted using a computerized universal testing machine named KIC-2-1000C produced by Kalpak Instruments & Controls, Pune. A constant crosshead speed of 5mm/min until failure of the sample is maintained. Figure 5 shows the tensile testing setup. Tensile test results clearly show the influence of the infill pattern on the strength of the specimens. The tensile strength of each infill pattern is affected by the geometry and the volume of material printed. The Tensile strength of the honeycomb infill pattern is greater than that of other infill patterns due to the higher volume of infill and the geometric shape of the honeycomb infill [31, 32]. It can therefore be concluded that, as a result of better stress distribution and load transfer for the honeycomb infill pattern, the tensile strength would increase when using a honeycomb infill print geometry [33]. Further, the concentric infill pattern records the maximum elongation prior to failure, and the cross-infill pattern shows the least elongation.

Equations 1 and 2 are used to compute the tensile strength and percentage elongation.

$$UTS = \frac{F_{max}}{A} \quad (1)$$

Where, F_{max} is the maximum applied force (N) and A is the cross-sectional area of the gauge section.

$$\%\ elongation = \left(\frac{L_f - L_o}{L_o}\right) x100 \quad (2)$$

Where, L_f represent the final gauge length after fracture and L_o is the original gauge length.

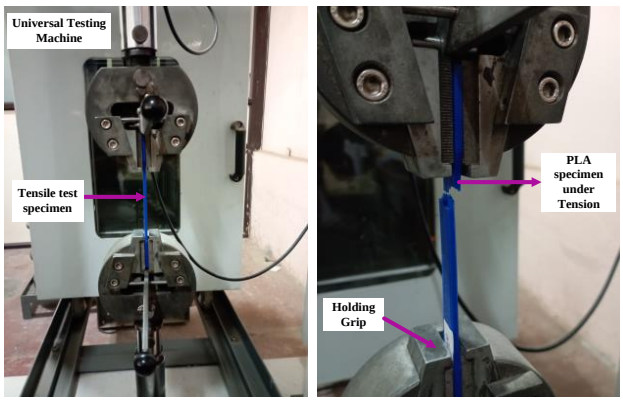

(a) **(b)**

Fig. 5 Tensile test setup for PLA specimen using UTM, (a) Full view showing specimen mounted in UTM grips, and (b) Close-up of specimen under axial tension during testing.

5.2. Flexural Test

ASTM D790 standard is used to perform flexural tests on the specimens prepared using FFF. Each sample measured 125 mm long x 12.7 mm wide x 3.2 mm thickness [34]. A total of 15 tests is conducted on 15 samples. Three – point bending mode is used in the universal testing machine to determine flexural strengths, percentage elongation and corresponding flexural modulus. Figure 6 shows flexural test sample subjected to transverse loading. The cross pattern exhibited the highest percentage elongation under bending indicating ability to *stretch more* before breaking.

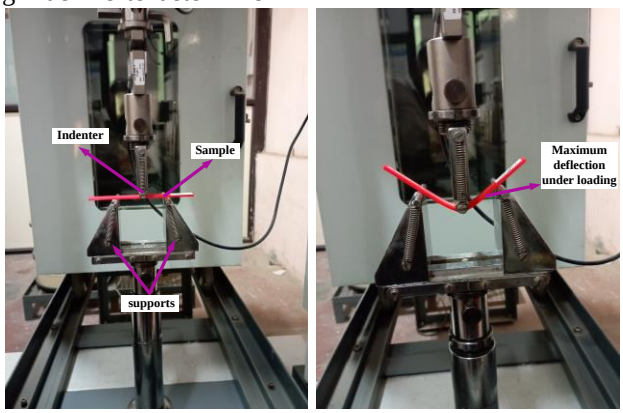

(a) **(b)**

Fig. 6 (a) Flexural test setup, and (b) Sample under maximum deflection during load application.

The following Equations (3-6) were used to calculate the flexural strength, modulus, and surface strain as per ASTM D790.

$$\sigma_f = \frac{3FL}{2bd^2} \quad (3)$$

Where, F = the load at fracture (N), L = support span length (mm), b = width of specimen (mm) and t = thickness of specimen (mm).

The stiffness of the material under bending was quantified using the following expression to determine the flexural modulus.

$$E_f = \frac{L^3 m}{4bd^2} \quad (4)$$

Where, m = slope of the load deflection curve.

The surface strain (percentage elongation) during flexural testing was obtained from the maximum central deflection using the equations below.

$$e_f = \frac{6Dd}{{L_s}^2} \quad (5)$$

$$\%\, elongation = e_f \times 100 \quad (6)$$

Where, D = maximum deflection at center which indicates the support span length.

6. Selection of Parameters and Application of RSM

6.1. Input and Output Parameters

To perform a systematic investigation using RSM, four key printing parameters were selected as input factors based on prior studies, machine limitations, and their known influence on the mechanical behavior of FFF PLA components. These parameters are the Density of Infill, Layer Height, Speed of Printing, and Temperature of the nozzle. The selection was made to capture the most impactful processing variables that govern the internal structure, interlayer bonding, and surface finish of FFF-printed parts.

The ranges for each parameter were chosen to balance mechanical performance with printability, while avoiding conditions that lead to structural failure or print defects. The selected input parameter ranges used in the Box-Behnken Design (BBD) are shown in Table 4.

Table 4. Input factors and levels of RSM

Factors	Symbol	Low Level (−1)	High Level (+1)	Unit
Infill Density	A	20%	50%	%
Layer Height	B	0.1	0.3	mm
Printing Speed	C	30	60	mm/s
Nozzle Temp.	D	190	220	°C

These input factors were varied according to the BBD matrix to develop predictive models for five key output responses. For tensile testing, the responses considered were Ultimate Tensile Strength (MPa) and Percentage Elongation (%).

For flexural testing, the responses included Flexural Strength (MPa), Bending Modulus (MPa), and Percentage Elongation (%). These outputs provide a wide understanding of the material strength, stiffness, and ductility, enabling the development of predictive models and optimization strategies through RSM.

6.2. Response Surface Methodology

RSM is used to study the interaction of the parameters considered. RSM allows for modelling, predicting, and optimizing through a systematic statistical design of experiments; thus, it provides the best means to identify the ideal settings to improve tensile and flexural properties [35].

To structure the experimental plan, a Box-Behnken Design (BBD) was selected. BBD is particularly suitable for fitting second-order models while minimizing the number of required experiments. It also avoids extreme factor combinations that might compromise print integrity [36]. Initial research into the honeycomb infill identified the honeycomb space as having the optimal configuration for maximum strength, which was later verified through laboratory testing. The experimental data generated from the work formed the basis for the RSM development and optimization methodology. Mathematical regression analysis is used to understand the relationship between the input and output parameters. It is a second-degree least squares polynomial that predicts the form and the impact of the input variables on the output variable response, Equation 7. Figure 7 shows the flow chart of RSM.

$$Y = \beta_0 + \sum \beta_i X_i + \sum \beta_{ii} X_i^2 + \sum \beta_{ij} X_i X_j \qquad (7)$$

Where, Y = Output responses, X_i = the input factors and β = coefficients.

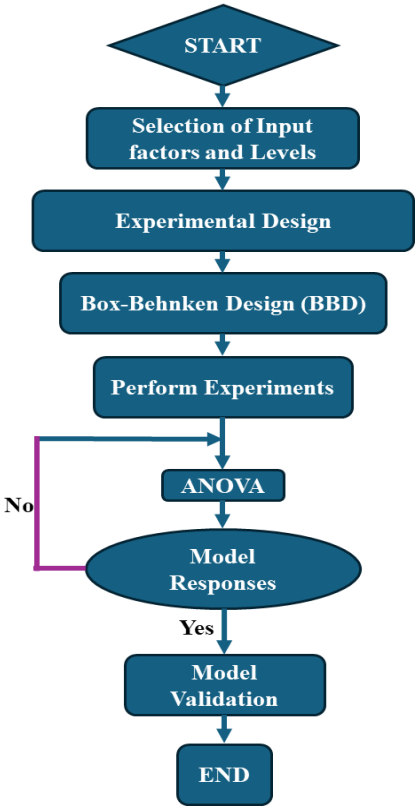

Fig. 7 Flow chart of RSM

The statistical analysis, including regression model development, Analysis of Variance (ANOVA), and the generation of three-dimensional surface plots, was conducted using Design Expert software. The objectives of applying RSM in this work were to identify the significant process parameters affecting tensile and flexural properties, to develop reliable predictive regression models for each mechanical response, and to determine the optimal parameter settings that yield the highest mechanical performance in 3D printed PLA parts [37].

7. Results and Discussions

7.1. Experimental Results

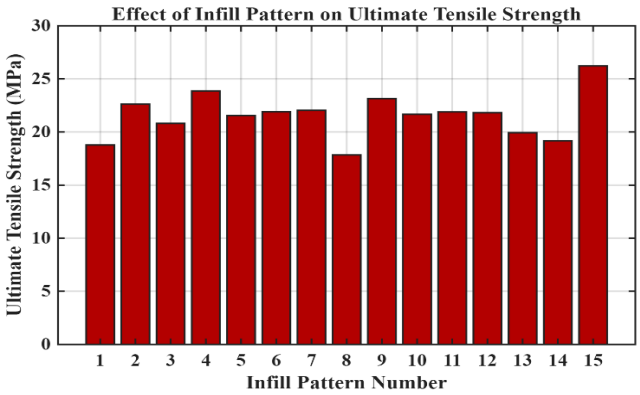

(a)

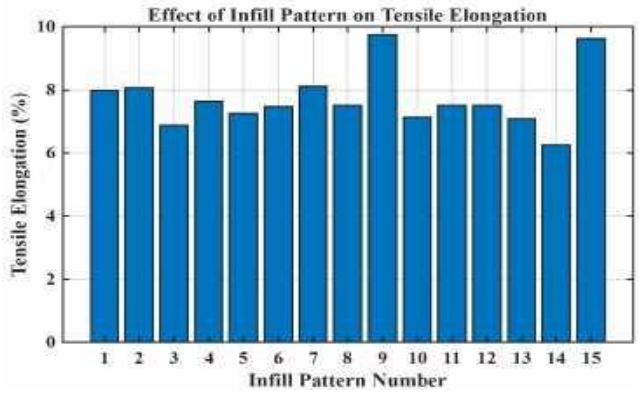

(b)

Fig. 8 Variation in, (a) Ultimate tensile strength and (b) Tensile elongation.

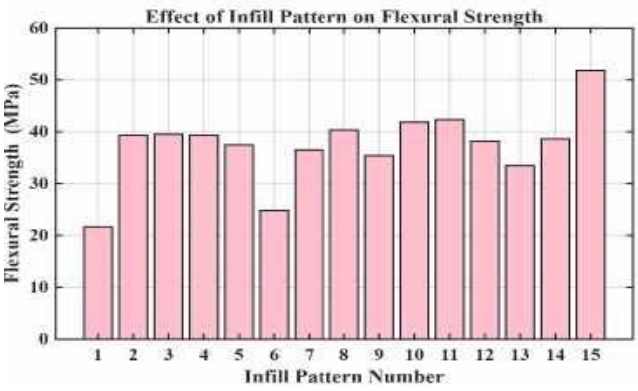

(a)

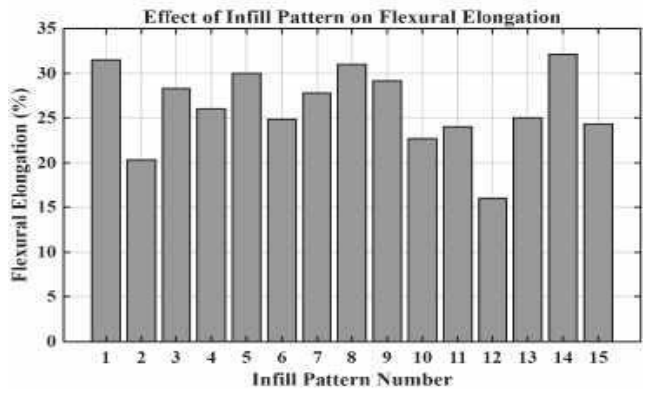

(b)

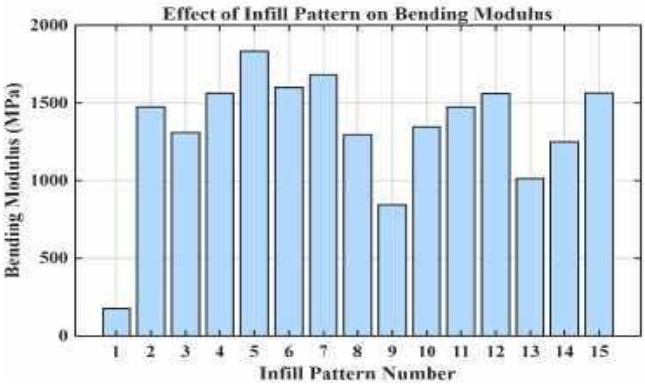

(c)

Fig. 9 Variation in, (a) Flexural strength, (b) Flexural elongation, and (c) Bending modulus.

Figures 8 (a) and 8 (b) show the ultimate tensile strength and tensile elongation of the fifteen different types of infill patterns considered in this study. With 26.22 MPa ultimate tensile strength, the honeycomb pattern demonstrates that this pattern provides the best arrangement of load-bearing. The concentric pattern had a similar amount of strength as the honeycomb pattern but was able to elongate a significant amount under tensile load, with a maximum elongation of 9.75%. Therefore, the concentric pattern provided greater ductility and ability to absorb energy than all other analyzed configurations. Other configurations did not provide adequate bonding between the layers; therefore, The honeycomb infill also showed the greatest flexural strength at 51.84 MPa, which also indicates that it can support bending loads well Figure 9 (a).

The cross-pattern demonstrated the most significant elongation under flexural load at 32.1%, providing significant flexibility, though not necessarily high strength, Figure 9 (b). Triangles and quarter-cubic infill patterns will also provide similar results with adequate elongation and supporting a relatively high rigidity. The triangles infill pattern had the highest bending Modulus at 1834 MPa, suggesting that it provides greater rigidity than any other pattern of infill used in this study Figure 9 (c). Overall, the honeycomb pattern of infill provides the optimum blend of strength, rigidity, and ductility, therefore being the best pattern of infill for all building applications where mechanical performance is most important.

7.2. Failure Analysis using SEM

The mechanisms of failure for 3D printed PLA tensile samples were identified through fractographic analysis using a SEM. This analysis provides insights into the microstructure of 3D printed samples regarding the bond between layers, fracture propagation, and defects within the sample that affect their mechanical performance based on the infill configuration.

Some of the failure modes observed in the SEM images of tensile tested samples, as shown in Figure 10**,** varied significantly depending on the infill pattern used; some of the images present the fracture surfaces with varying amounts of layer separation and delamination due to insufficient bonding between layers of material that had been previously extruded as well as void spaces which create areas of stress concentration during loading for tensile testing particularly in sample patterns with a low amount of overlap for material. In some regions, both translational and brittle fractures occurred, with relatively sharp and defined edges usually corresponding to low-performing infill configurations. Conversely, the regions of plastic deformation became readily apparent in the honeycomb configuration, indicating that the honeycomb configuration provided energy-absorbing characteristics due to the high degree of continuity between the fractures produced by the filaments throughout the tensile testing. A higher concentration of fused and compacted layers in the high-performing pattern samples was highly correlated with the experimental tensile testing results, in which the honeycomb pattern exhibited superior strength and elongation; however, the other patterns produced lower cohesive fracture surfaces with poor adherence between filament layers and contained more voids, resulting in early failure.

7.2.1. Tensile Failure Characteristics

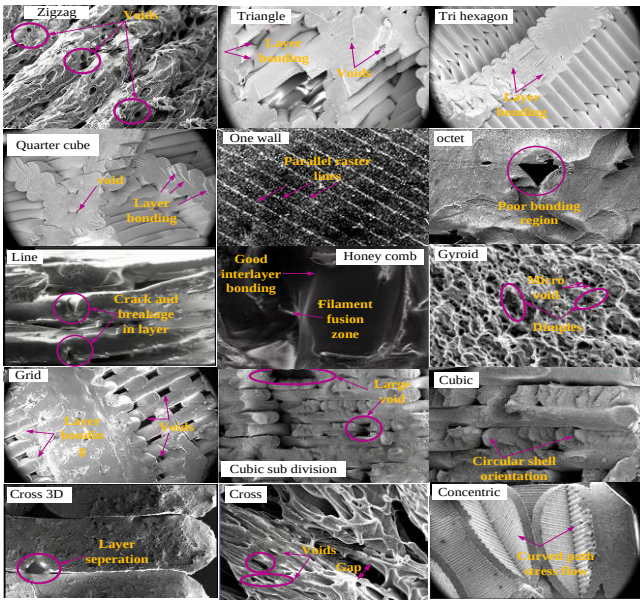

Fig. 10 SEM images showing typical tensile fracture surfaces for all infill patterns

7.2.2. Flexural Failure Characteristics-Literature-Based Interpretation

Although SEM imaging was not performed on samples tested under flexural loading, their failure can be discussed on previous literature. During Flexural testing lower surface of experiences the tensile stress and the upper surface with the compressive stress thus it results in asymmetric fracture surfaces [37]. Failure generally initiates at the tensile surface, especially in patterns with weak interlayer bonding, which leads to crack initiation and propagation across the print layers [38]. On the compressive side, buckling or wrinkling of the filament structure may occur, which is less visible externally but contributes to sudden structural collapse [39]. High-performance infill patterns such as Honeycomb, which demonstrated more flexural strength and elongation, likely resisted deformation through more uniform internal support and better stress distribution [40]. This combination of empirical and microstructural understanding helps in identifying the failure modes which helps improving the design of components developed using FFF technique for specific loading conditions.

7.3. RSM Analysis

Table 5. RSM experimental results

		Factor 1	Factor 2	Factor 3	Factor 4	Response 1	Response 2	Response 1	Response 2	Response 3
Std	**Run**	**A: Infill Density**	**B: Printing Speed**	**C: Layer Height**	**D: Nozzle Temperature**	**Ultimate Tensile Strength**	**Percentage Elongation (Tensile)**	**Flexural Strength**	**Bending Modulus**	**Percentage Elongation (Flexural)**
		%	mm/s	mm	°C	MPa	%	MPa	MPa	%
11	1	20	60	0.2	220	17.81	5.80	36.5	1032.6	25.7
17	2	20	60	0.1	210	21.10	7.30	36.3	1346.8	25.0
2	3	60	40	0.2	210	21.60	7.50	23.8	454.1	17.0
21	4	40	40	0.2	200	21.50	7.40	41.5	1398.8	28.6
19	5	20	60	0.3	210	22.40	8.00	33.5	983.5	24.8
30	6	40	60	0.2	210	23.80	8.30	41.6	1528.2	29.1
7	7	40	60	0.1	220	21.30	7.72	27.5	854.1	23.3
23	8	30	40	0.2	220	20.42	6.98	41.5	1478.1	29.0
22	9	40	80	0.2	200	23.40	8.10	33.7	1107.2	28.0
10	10	60	60	0.2	200	21.11	7.33	42.0	1445.4	29.3
1	11	20	40	0.2	210	21.47	7.50	33.9	1165.8	29.8
8	12	40	60	0.3	220	22.90	7.66	45.8	1722.3	32.6
24	13	40	80	0.2	220	22.03	7.50	37.1	1330.4	29.6
16	14	30	80	0.3	210	22.49	7.89	38.8	1408.9	27.4
14	15	40	80	0.1	210	23.33	8.05	39.9	1569.6	29.4
13	16	40	40	0.1	210	21.10	7.71	34.0	1259.3	27.8
28	17	40	60	0.2	210	23.56	8.25	42.6	1503.2	28.4
27	18	40	60	0.2	210	23.99	8.31	43.6	1657.6	30.7
29	19	40	60	0.2	210	24.32	8.48	38.5	1503.7	32.0
20	20	60	60	0.3	210	24.63	8.45	41.1	1215.2	27.1
4	21	60	80	0.2	210	24.86	8.84	43.7	1761.6	30.5
9	22	20	60	0.2	200	25.06	9.03	48.6	1783.6	32.8
3	23	20	80	0.2	210	20.90	7.20	42.7	1524.8	28.8
15	24	40	40	0.3	210	23.00	7.69	34.9	947.6	22.4
26	25	40	60	0.2	210	23.80	8.56	40.6	1549.4	33.7
6	26	30	60	0.3	200	23.40	8.20	42.4	1775.6	27.6
25	27	40	60	0.2	210	23.80	8.43	51.3	1773.4	33.6
18	28	60	60	0.1	210	24.80	9.58	41.6	1524.8	28.3
12	29	60	60	0.2	220	26.36	9.62	41.6	1478.1	32.7
5	30	40	60	0.1	200	24.10	8.50	39.7	1400.9	23.6

7.3.1. ANOVA for All Responses

The ANOVA results confirm the statistical soundness of RSM models developed for all five mechanical response variables, ultimate tensile strength, tensile percentage elongation, flexural strength, bending Modulus, and flexural percentage elongation. High F-value along with the low p-value ($p < 0.0001$), indicating that the regression models are highly significant. This indicates that variation in responses is strongly affected by the selected process parameters, which are the density of infill, printing layer height, speed of printing, and temperature of the nozzle. In addition, the lack-of-fit values for all responses are found to be statistically non-significant. Table 6 shows the ANOVA for all responses. This suggests that the models represent experimental data

adequately and there is no substantial variation left unexplained by the fitted models. The models capture the actual behavior of the system without overfit. These outcomes demonstrate that the RSM approach applied in this study is valid and effective for estimating and optimizing the performance of the components fabricated using the FFF technique.

Table 6. ANOVA for all responses

Responses	F-value	p-value	Model	Lack of Fit
Ultimate Tensile strength	67.56406	< 0.0001	significant	not significant
percentage elongation (Tensile)	25.01867	< 0.0001	significant	not significant
flexural strength	62.61	< 0.0001	significant	not significant
bending Modulus	59.98699	< 0.0001	significant	not significant
percentage elongation (flexural)	23.70024	< 0.0001	significant	not significant

7.3.2. Fit Statistics for All Responses

The fit statistics confirm that the developed RSM models are both accurate and reliable. All responses show high R^2 values (≥ 0.95), indicating predicted and experimental results are almost the same Table **7**. The models' good Predictive capability without overfitting is observed by the with close values obtained for adjusted R^2 and predicted R^2. All of models' Adequate Precision values are well above 4 (indicating a high signal-to-noise ratio) and demonstrate that they can be successfully utilized to navigate the design space. The models are statistically reliable and efficient at providing optimized mechanical performance for 3D printing PLA components.

Table 7. Fit statistics for all responses

Responses	Std. Dev.	R^2	Adjusted R^2	Predicted R^2	Adeq Precision
Ultimate Tensile strength	0.3064	0.9844	0.9698	0.9257	37.5082
percentage elongation (Tensile)	0.1449	0.9818	0.9649	0.9140	37.5082
flexural strength	1.0188	0.9831	0.9674	0.9109	36.6646
bending modulus	56.8452	0.9824	0.9660	0.9161	34.7392
percentage elongation (flexural)	1.0613	0.9567	0.9163	0.9072	22.2993

7.3.3. Perturbation Plot

The sensitivity of mechanical properties to process parameters such as infill density (A), print speed (B), layer height (C), and nozzle temperature (D) for 3D printed PLA parts is presented in Figures 11 and 12 as perturbation plots. In the case of ultimate tensile strength and tensile elongation, increasing infill density has a strong positive effect — both tensile strength and tensile elongation increase as the infill density increases; conversely, higher nozzle temperatures will have a negative effect on both tensile strength and tensile elongation. For flexural strength and flexural elongation, layer height (C) and infill density (A) are more influential, with moderate increases improving the properties. In the case of bending Modulus, infill density (A) Again shows the most substantial positive impact, indicating its important role in increasing structural rigidity. These plots clearly show that out of four parameters, the infill density has the clearest effect on continuous mechanical behavior, which confirms its importance in optimization of FFF-printed PLA parts.

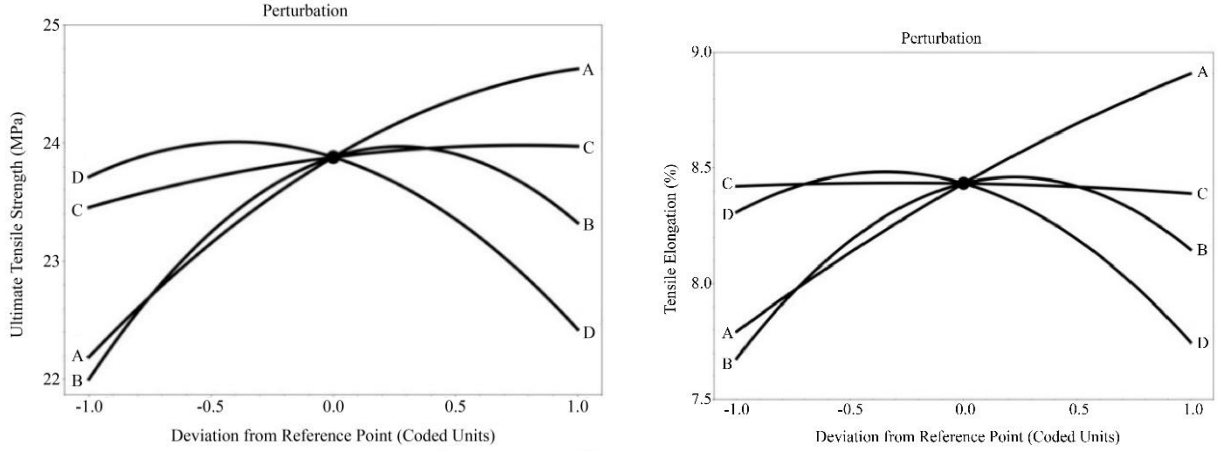

(a) **(b)**

Fig. 11 Perturbation plot of, (a) Tensile strength, and (b) Tensile.

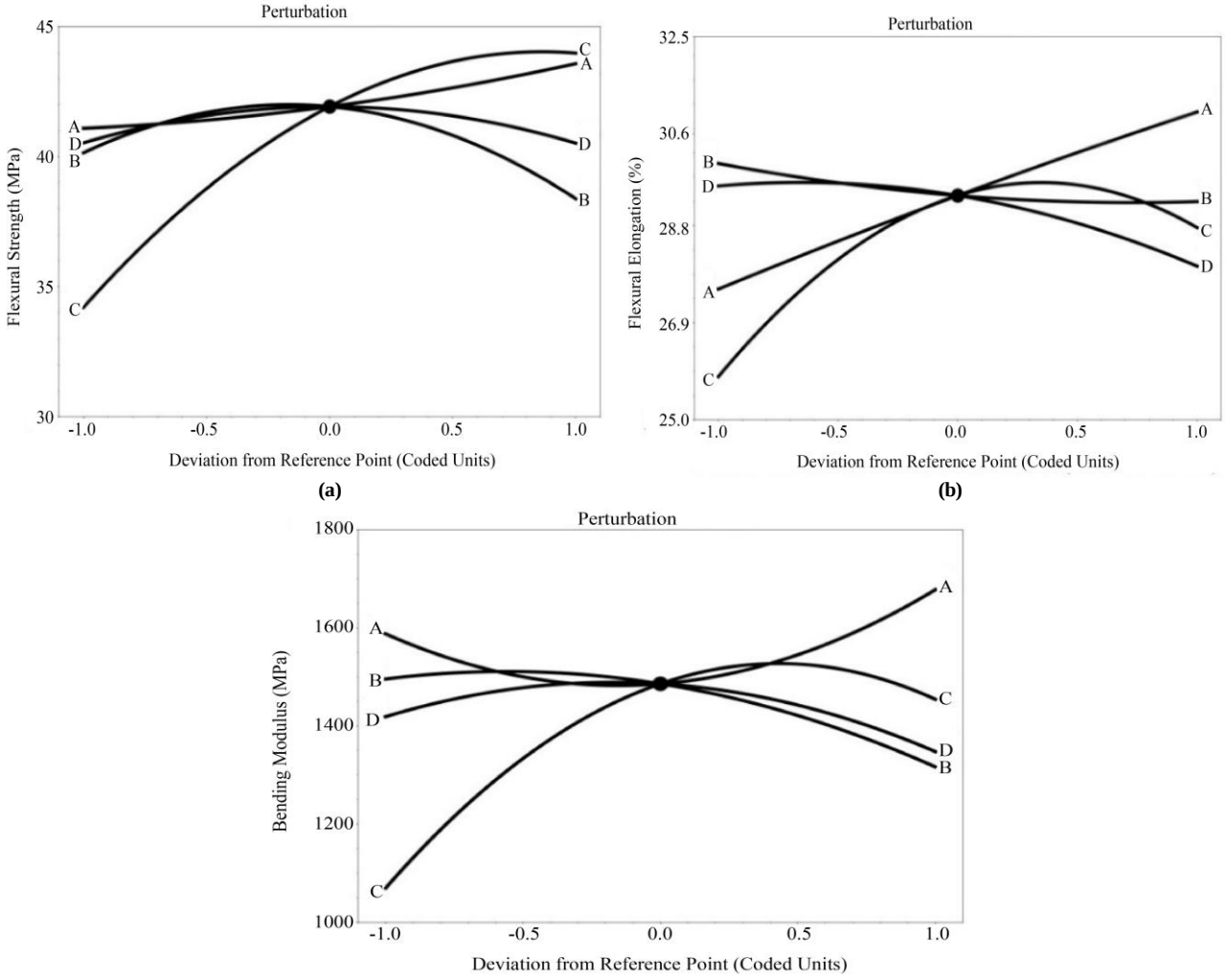

Fig. 12 Perturbation plot of, (a) Flexural strength, (b) Flexural elongation, and (c) Bending modulus.

7.3.4. 3D Contour Plot

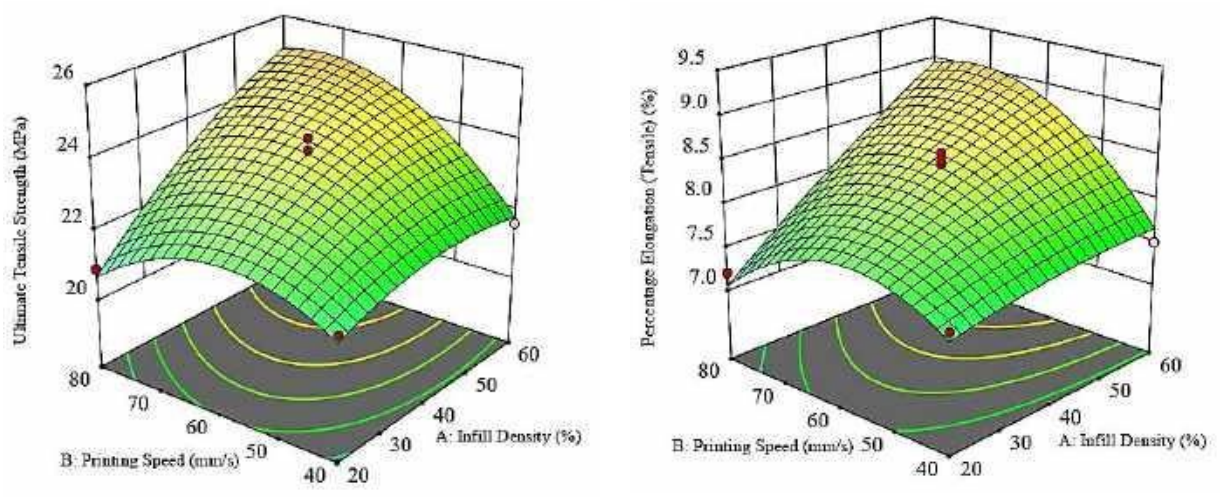

Fig. 13 3D Contour plot of, (a) Tensile strength, and (b) Tensile elongation.

The 3D plots of the response surfaces illustrate the interactive influences of infill density and printing speed for the mechanical performance of FFF printed PLA parts in Figure 13. Figures 13 (a) and 13 (b) both show that ultimate tensile strength and tensile elongation exhibit a nonlinear response with respect to the initial increase in infill density, increasing ductility and strength up to a peak, after which they decline at extremely high print speeds or densities due to thermal inconsistencies or insufficient bond strength between layers. Figures 14 (a) and 14 (b) display similar trends for flexural strength and bending Modulus, where moderate infill (around 40–60%) and intermediate printing speeds (50–60 mm/s) lead to optimal bending performance. Figure 14 (c) shows that flexural elongation steadily improves with increasing infill density and decreases only slightly at higher speeds. These surface plots validate the optimization ranges and emphasize the critical role of balancing material fill and printing rate for enhancing both tensile and flexural characteristics of printed PLA components.

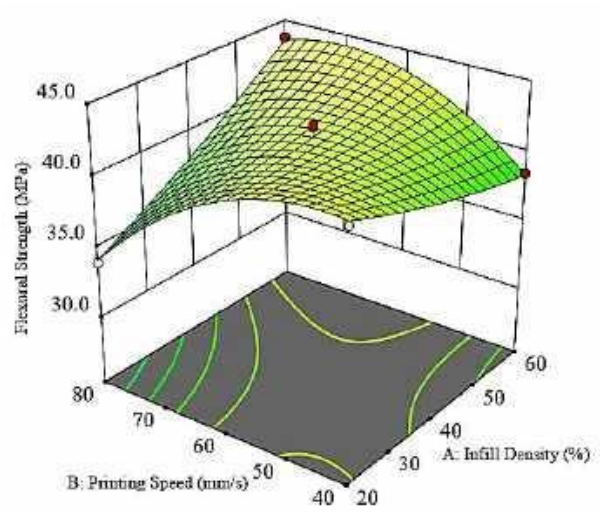

(a)

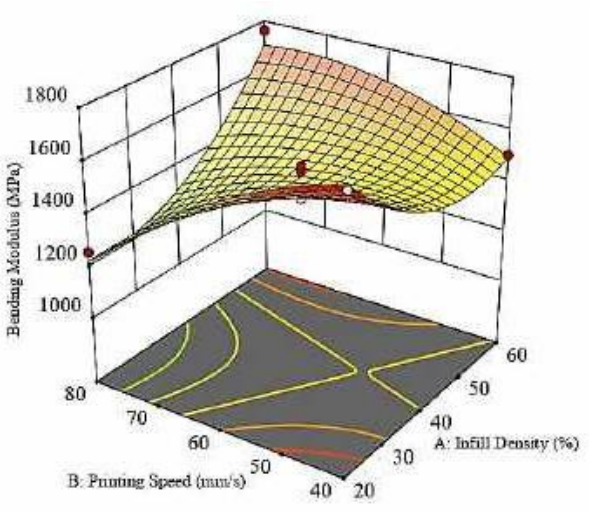

(b)

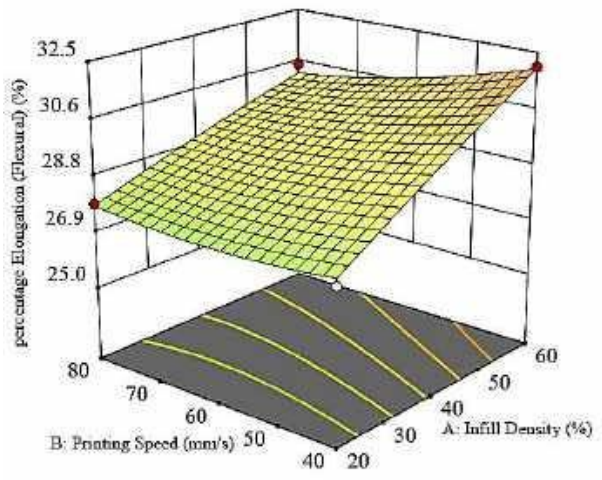

(c)

Fig. 14 3D contour plot of, (a) Flexural strength, (b) Flexural elongation, and (c) Bending modulus.

7.3.5. Desirability Analysis

Figure 15 displays a desirability plot for optimization of the FFF Process Parameters using multiple objectives, in order to achieve the maximum mechanical performance. The optimized parameters ultimately yield optimal mechanical performance when the infill density is 30%, printing speed is 75.43 mm/s, height of each layer is 0.1029 mm, and temperature of the nozzle is 218.74 °C. This set produces the most desirable balance of all mechanical performance characteristics through the predicted ultimate tensile strength (26.57 MPa), elongation at 10.04%, flexural strength (52.2 MPa), flexural Modulus (1912.8 MPa), and flexural elongation (35.5%). All of these properties are near their respective upper limits; thus, all represent optimal mechanical performance. The overall desirability of the

parameter set (R^2) is 0.960, indicating that this is an excellent overall compromise for all mechanical properties. This result demonstrates the benefit of applying Response Surface Methodology (RSM) to process optimization.

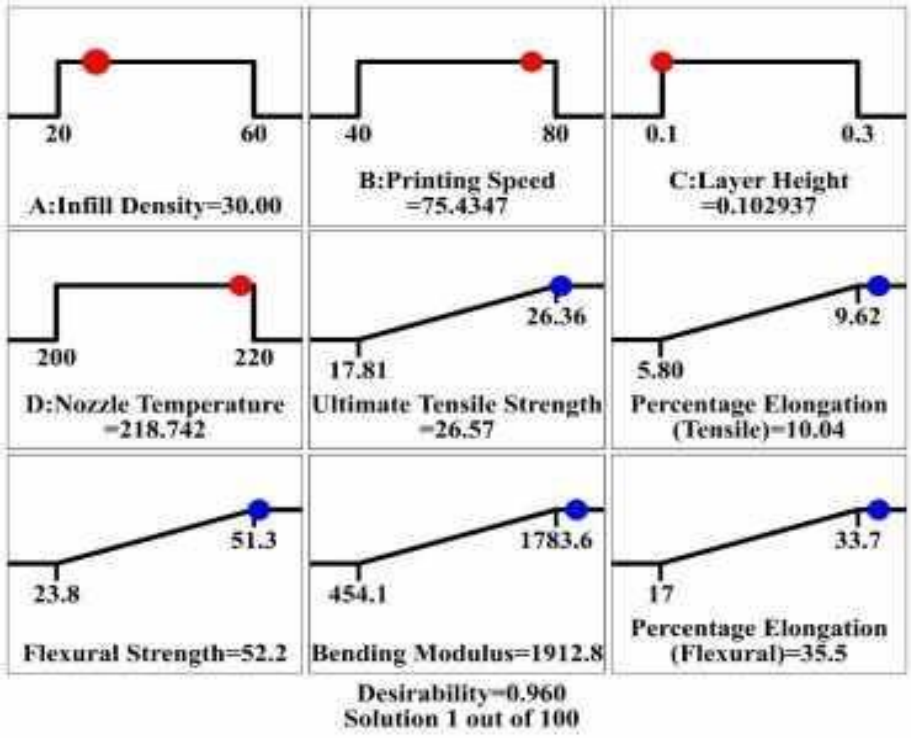

Fig. 15 RSM optimized desirability plot

8. Conclusion

The current study carefully examines fifteen different infill patterns produced using the FFF technique and PLA material for their effect on the mechanical properties. In addition to physical testing, RSM was used to establish the optimum four parameters (density of infill, layer height, speed of printing, and temperature of nozzle) in order to increase their performance properties. SEM was substantiated as a complementary tool to establish the mode (mechanism) of failure in the selected infill patterns. Findings from this study provide valuable references to improve the mechanical strength of 3D-printed parts used in engineering applications (i.e., construction).

- Of the fifteen infill patterns tested, the results indicate that the honeycomb infill pattern provided the best performance of all configurations tested. The honeycomb pattern yielded the highest mechanical properties (e.g., ultimate tensile strength = 26.22 MPa; elongation at tensile breaking = 9.62%; flexural strength = 51.84 MPa; bending Modulus = 1562.71 MPa; elongation at flexural breaking = 24.31%).
- The use of RSM to optimise parameter settings was successful in identifying the optimum process parameters (30% infill density, 75.43 mm/s print speed, 0.1029 mm layer height, and 218.74°C nozzle temperature) that resulted in the highest desired mechanical properties.
- The RSM model produced a maximum desirability of 0.960, indicating a strong prediction and concurrent optimization capability for multiple mechanical outputs.

SEM analysis of these samples confirmed the RSM predictions with improved bonding between the filament, fewer voids, and improved cohesion of the fracture surface area of honeycomb samples, thus providing supporting evidence for the mechanical superiority of the honeycomb configuration.

References

[1] P. Arunkumar et al., "Effect of Infill Pattern on Mechanical Properties of 3D Printed PLA-Zn Composites for Drone Frame Structures: A Topology Optimization Integrated Application Study," *Results in Engineering*, vol. 25, pp. 1-9, 2025. [CrossRef] [Google Scholar] [Publisher Link]

[2] Mehrnoosh Javadian et al., "Fatigue Behavior and Failure Mechanism of 3D-printed Continuous Glass Fiber-Reinforced PLA Composites under Rotating Bending Fatigue," *Composites Part C: Open Access*, vol. 17, pp. 1-13, 2025. [CrossRef] [Google Scholar] [Publisher Link]

[3] Salethkumar Jasper et al., "Effect of Infill Pattern on the Microstructure and Properties of Copper Processed through Metal Fused Filament Fabrication Technique," *Journal of Materials Research and Technology*, vol. 35, pp. 2791-2802, 2025. [CrossRef] [Google Scholar] [Publisher Link]

[4] Lea Strauß et al., "An Equivalent Stress Approach for Predicting Fatigue Behavior of Additively Manufactured AlSi10Mg," *Progress in Additive Manufacturing*, vol. 10, pp. 3071-3086, 2025. [CrossRef] [Google Scholar] [Publisher Link]

[5] Rajan Narang et al., "Optimization of Process Parameters to Investigate the Fatigue Behavior of Fused Deposition Modeling-Fabricated ABS Parts Using Hybrid Tool," *Journal of Materials Engineering and Performance*, vol. 34, pp. 23045-23058, 2025. [CrossRef] [Google Scholar] [Publisher Link]

[6] J.M. Cañero-Nieto et al., "Infill Pattern Strategy Impact on the Cross-Sectional Area at Gauge Length of Material Extrusion 3D Printed Polylactic Acid Parts," *Journal of Intelligent Manufacturing*, pp. 1-22, 2025. [CrossRef] [Google Scholar] [Publisher Link]

[7] Sumit Singh, Rajesh Kumar Attri, and Shefali Trivedi, "Taguchi-based Optimization for Tensile Strength in FDM Printed Nano-Graphene-Reinforced PLA Components," *The International Journal of Advanced Manufacturing Technology*, 2025. [CrossRef] [Google Scholar] [Publisher Link]

[8] Nikhil Bharat et al., "Influence of 3D Printing FDM Process Parameters on Compressive Strength of PLA/Carbon Fiber Composites: ANOVA and Backpropagation Neural Network Approach," *Journal of Materials Engineering and Performance*, vol. 34, pp. 20830-20843, 2025. [CrossRef] [Google Scholar] [Publisher Link]

[9] S. Ganeshkumar et al., "Investigation of Tensile Properties of Different Infill Pattern Structures of 3d-Printed PLA Polymers: Analysis and Validation Using Finite Element Analysis in ANSYS," *Materials*, vol. 15, no. 15, pp. 1-11, 2022. [CrossRef] [Google Scholar] [Publisher Link]

[10] Jibran Khaliq, Dharma Raj Gurrapu, and Farah Elfakhr, "Effects of Infill Line Multiplier and Patterns on Mechanical Properties of Lightweight and Resilient Hollow Section Products Manufactured Using Fused Filament Fabrication," *Polymers*, vol. 15, no. 12, pp. 1-14, 2023. [CrossRef] [Google Scholar] [Publisher Link]

[11] Miguel Fernandez-Vicente et al., "Effect of Infill Parameters on Tensile Mechanical Behavior in Desktop 3D Printing," *3D Printing and Additive Manufacturing*, vol. 3, no. 3, pp. 183-192, 2016. [CrossRef] [Google Scholar] [Publisher Link]

[12] Faisal J. Alzahrani et al., "A Comprehensive Investigation of Infill Geometry Effects on the Mechanical Performance of Polymer 3D Printed Components," *Polymers*, vol. 18, no. 1, pp. 1-11, 2025. [CrossRef] [Google Scholar] [Publisher Link]

[13] Tanner David Harpoo et al., "Evaluation of the Infill Design on the Tensile Response of 3D Printed Polylactic Acid Polymer," *Materials*, vol. 14, no. 9, pp. 1-20, 2021. [CrossRef] [Google Scholar] [Publisher Link]

[14] Vasile Cojocaru, Doina Frunzaverde, and Calin-Octavian Miclosina, "On the Behavior of Honeycomb, Grid and Triangular PLA Structures under Symmetric and Asymmetric Bending," *Micromachines*, vol. 14, no. 1, pp. 1-18, 2022. [CrossRef] [Google Scholar] [Publisher Link]

[15] Yasith S. Perera et al., "Investigation of the Mechanical Properties of 3D Printed Hollow Parts with Finite Element Analysis," *Journal of Materials Research and Technology*, vol. 36, pp. 8826-8839, 2025. [CrossRef] [Google Scholar] [Publisher Link]

[16] Ömer Çerlek et al., "Experimental Investigation of Parameters Affecting the Tensile Strength of Silicone-Filled 3D Printed ABS Products," *Journal of Materials Engineering and Performance*, vol. 34, pp. 9627-9636, 2025. [CrossRef] [Google Scholar] [Publisher Link]

[17] Anant Prakash Agrawal et al., "An Investigation of Combined Effect of Infill Pattern, Density, and Layer Thickness on Mechanical Properties of 3D Printed ABS by Fused Filament Fabrication," *Heliyon*, vol. 9, no. 6, pp. 1-12, 2023. [CrossRef] [Google Scholar] [Publisher Link]

[18] Daniyar Syrlybayev et al., "Optimisation of Strength Properties of FDM Printed Parts—A Critical Review," *Polymers*, vol. 13, no. 10, pp. 1-35, 2021. [CrossRef] [Google Scholar] [Publisher Link]

[19] Mohammadreza Lalegani Dezaki, and Mohd Khairol Anuar Mohd Ariffin, "The Effects of Combined Infill Patterns on Mechanical Properties in FDM Process," *Polymers*, vol. 12, no. 12, pp. 1-20, 2020. [CrossRef] [Google Scholar] [Publisher Link]

[20] H. Gonabadi, A. Yadav, and S. J. BullB, "The Effect of Processing Parameters on the Mechanical Characteristics of PLA Produced by a 3D FFF Printer," *The International Journal of Advanced Manufacturing Technology*, vol. 111, pp. 695-709, 2020. [CrossRef] [Google Scholar] [Publisher Link]

[21] Shrikant Bardiya, J. Jerald, and V. Satheeshkumar, "The Impact of Process Parameters on the Tensile Strength, Flexural Strength and the Manufacturing Time of Fused Filament Fabricated (FFF) Parts," *Materials Today: Proceedings*, vol. 39, pp. 1362-1366, 2021. [CrossRef] [Google Scholar] [Publisher Link]

[22] Shivani Sriya Ambati, and Ravindra Ambatipudi, "Effect of Infill Density and Infill Pattern on the Mechanical Properties of 3D Printed PLA Parts," *Materials Today: Proceedings*, vol. 64, pp. 804-807, 2022. [CrossRef] [Google Scholar] [Publisher Link]

[23] Mohamed Hamoud et al., "Investigating the Influence of 3D Printing Parameters on the Mechanical Characteristics of FDM Fabricated (PLA/Cu) Composite Material," *The International Journal of Advanced Manufacturing Technology*, vol. 134, pp. 3769-3785, 2024. [CrossRef] [Google Scholar] [Publisher Link]

[24] Mustafa Özgür Öteyaka, Kerem Aybar, and Hasan Candan Öteyaka, "Effect of Infill Ratio on the Tensile and Flexural Properties of Unreinforced and Carbon Fiber-Reinforced Polylactic Acid Manufactured by Fused Deposition Modeling," *Journal of Materials Engineering and Performance*, vol. 30, pp. 5203-5215, 2021. [CrossRef] [Google Scholar] [Publisher Link]

[25] Amir Khodaee, Vahid Abedini, and Abdolvahed Kami, "Effects of Fused Filament Fabrication (FFF) Process Parameters on Tensile and Flexural Properties of ABS/PLA Multi-Material," *Journal of the Brazilian Society of Mechanical Sciences and Engineering*, vol. 46, 2024. [CrossRef] [Google Scholar] [Publisher Link]

[26] Márton Tamás Birosz, and Mátyás Andó, "Effect of Infill Pattern Scaling on Mechanical Properties of FDM-Printed PLA Specimens," *Progress in Additive Manufacturing*, vol. 9, pp. 875-883, 2024. [CrossRef] [Google Scholar] [Publisher Link]

[27] Muthuselvan Balasubramanian et al., "Exploring the Synergistic Influence of FDM Parameters and Strain Rate on Tensile Strength and Failure Mechanism of FDM Printed PLA," *Progress in Additive Manufacturing*, vol. 10, pp. 2765-2774, 2025. [CrossRef] [Google Scholar] [Publisher Link]

[28] RajeshKumar Dhanapal, Vasudevan Alagumalai, and Vigneshwaran Shanmugam, "Exploring the Dynamic Mechanical Properties of Fused Filament Fabrication Printed Polyetheretherketone with Various Infill Patterns," *Progress in Additive Manufacturing*, vol. 10, pp. 2911-2926, 2025. [CrossRef] [Google Scholar] [Publisher Link]

[29] Logesh Kothandaraman et al., "Mechanical Characterization of Planar PLA/CF Composites with Cell-sized Structures using Fused Filament Fabrication," *Progress in Additive Manufacturing*, vol. 10, pp. 9459-9473, 2025. [CrossRef] [Google Scholar] [Publisher Link]

[30] Akshay S. Karad et al., "Experimental Study of Effect of Infill Density on Tensile and Flexural Strength of 3D Printed Parts," *Journal of Engineering and Applied Science*, vol. 70, pp. 1-17, 2023. [CrossRef] [Google Scholar] [Publisher Link]

[31] Seshaiah Turaka et al., "Impact of Infill Density on Morphology and Mechanical Properties of 3D Printed ABS/CF-ABS Composites using Design of Experiments," *Heliyon*, vol. 10, no. 9, pp. 1-26, 2024. [CrossRef] [Google Scholar] [Publisher Link]

[32] Jingjing Liu et al., "Effect of Infill Parameters on the Compressive Strength of 3D-Printed Nylon-Based Material," *Polymers*, vol. 15, no. 2, pp. 1-19, 2023. [CrossRef] [Google Scholar] [Publisher Link]

[33] Mateus Q. Dos Reis et al., "Effect of the Infill Density on 3D-Printed Geometrically Graded Impact Attenuators," *Polymers*, vol. 16, no. 22, pp. 1-16, 2024. [CrossRef] [Google Scholar] [Publisher Link]

[34] Hossein Afshari et al., "Studying the Effects of FDM Process Parameters on the Mechanical Properties of Parts Produced from PLA using Response Surface Methodology," *Colloid and Polymer Science*, vol. 302, pp. 955-970, 2024. [CrossRef] [Google Scholar] [Publisher Link]

[35] Abhishek Raj et al., "Optimizing the Process Parameters with Statistical and Soft Computing Techniques for Enhanced Mechanical Properties of Acrylonitrile Butadiene Styrene Material Samples Fabricated via Fused Filament Fabrication Technique," *Progress in Additive Manufacturing*, vol. 10, pp. 2559-2583, 2025. [CrossRef] [Google Scholar] [Publisher Link]

[36] Fikadu Mequant Kidie, Tesfa Guadie Ayaliew, and Samuel Tesfaye Mekonone, "Optimizing 3D Printing Process Parameters to Improve Surface Quality and Investigate the Microstructural Characteristics of PLA Material," *The International Journal of Advanced Manufacturing Technology*, vol. 138, pp. 457-470, 2025. [CrossRef] [Google Scholar] [Publisher Link]

[37] S. Santosh, M. Siranjith Sujan Muthiah, and K. Sriram Nishad, "Influence of Infill Density on the Mechanical Properties and Fracture Behavior of 3D-printed PLA + Components," *Macromolecular Research*, Res, vol. 33, pp. 1407-1420, 2025. [CrossRef] [Google Scholar] [Publisher Link]

[38] Siddharth Garg, Aditya Singh, and Qasim Murtaza, "Measuring the Impact of Infill Pattern and Infill Density on the Properties of 3D-Printed PLA via FDM," *Journal of Materials Engineering and Performance*, vol. 34, pp. 22597-22610, 2025. [CrossRef] [Google Scholar] [Publisher Link]

[39] R. Rajiev, S. Saravanan, and R. Rajkumar, "Assessing Surface Quality with SEM Analysis and Evaluating the Parameters and Mechanical Properties of PLA Parts Produced by 3D Printing," *Interactions*, vol. 246, 2025. [CrossRef] [Google Scholar] [Publisher Link]

[40] Dikshita Chowdhury, and Sunhee Lee, "Study on the Various Lightweight PLA Honeycomb Structures with 3D Printing Process Conditions," *Fashion and Textiles*, vol. 12, pp. 1-19, 2025. [CrossRef] [Google Scholar] [Publisher Link]